ACS OMEGA

http://pubs.acs.org/journal/acsodf

Article

Synthesis of Chitosan/Diatomite Composite as an Advanced Delivery System for Ibuprofen Drug; Equilibrium Studies and the Release Profile

Sherouk M. Ibrahim, May N. Bin Jumah, Sarah I. Othman, Reem Saleh Alruhaimi, Nora Al-Khalawi, Yasser F. Salama, Ahmed A. Allam, and Mostafa R. Abukhadra*

Cite This: *ACS Omega* 2021, 6, 13406−13416

Read Online

ACCESS | Metrics & More | Article Recommendations | Supporting Information

ABSTRACT: Chitosan/diatomite nanocomposite (CS/D) was synthesized as a low-cost and highly porous structure of enhanced physicochemical properties to be applied as advanced carriers for ibuprofen drug (IB). The loading properties of CS/D were studied in comparison to diatomite as a separated phase and achieved a loading capacity of 562.6 mg/g. The loading reactions of IB into CS/D show pseudo-second-order kinetic behavior and Langmuir isotherm properties. This demonstrates homogeneous loading processes in monolayer forms and controlled essentially by physical mechanisms. This was confirmed by the calculated Gaussian energy (7.7 kJ/mol (D) and 7.9 kJ/mol (CS/D)) in addition to the thermodynamic parameters. The thermodynamic behavior for the IB loading process is related to spontaneous, favorable, and exothermic reactions. The CS/D composite is of promising IB release profile that extended to about 200 h with a maximum release of 91.5% at the gastric fluid (pH 1.2) and 97.3% in the intestinal fluid (pH 7.4). The IB release rate from CS/D can be controlled based on the ratio of the integrated chitosan in the composite. The IB release reactions from CS/D follow the assumption of Korsmeyer−Peppas kinetics with determined values for the diffusion exponent reflects complex diffusion and erosion as the affected mechanisms during the IB release process.

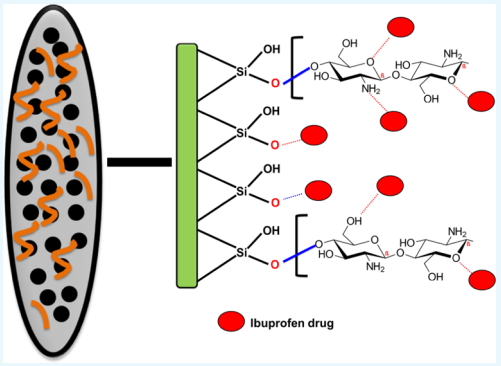

1. INTRODUCTION

Inflammation refers to the response of biological organisms to different infections, which might cause more damages than the main infection.[1,2] Several drugs such as azithromycin, ibuprofen, and levofloxacin were used to decline such inflammations effects.[3,4] Ibuprofen (IB) is a widely applied anti-inflammatory drug that has analgesic properties for musculoskeletal disorders and rheumatoid arthritis.[5] The normal use of ibuprofen faces significant challenges in the medical society due to its fast degradation properties (3.5 as half-life), poor bioavailability, low solubility, and high permeability.[6] The low dissolution rate has a strong negative influence in declining the bio-absorption of IB molecules into the bloodstream.[6] Additionally, other pernicious effects such as gastroschisis, cardiac septal abnormalities, and toxic impacts were reported for the uncontrolled overdose of the used IB drug.[7]

Interested researchers have developed several methods to enhance the stability; bio-distribution, solubility, and selectivity of the IB drug in addition to the role of such techniques in controlling the released dosages of the drug, improving the patient compliance, and inducing its therapeutic efficiency.[8−10] Introducing the drug at gradual delivery, managed dose, aggressively pursued, and targeted delivery using innovative carriers were recommended as promising methods to avoid all of the reported side effects.[1,9,10] The studied carriers for the IB drug involved mesoporous silica, hydroxyapatite, montmorillonite, titanium alloy, and MOFs.[5,6,11]

The selection of a suitable or a more effective drug carrier depends on the loading capacity, release rate, biocompatibility of the product, safety, and production cost.[12] The mesoporous forms of silica (MCM-41, MCM-48, and SBA-15) were studied extensively as promising drug delivery systems for different species of drugs.[13] They are biocompatible materials that have high loading capacities, and the polarity of their surfaces facilitates the dissolution of the loaded drug into the bloodstream.[14] Unfortunately, the high production cost of the synthetic porous silica and the toxicity of some of their raw materials in addition to its production time make them unfavorable for the commercial and industrial scales.

Natural nanoporous silica and silicate materials such as diatomite and natural zeolite can represent ideal alternatives

Received: March 21, 2021
Accepted: April 28, 2021
Published: May 13, 2021

for synthetic products as they are of similar siliceous porous structure and physicochemical properties, but they are less expensive.[15,16] Diatomite is a siliceous sedimentary rock that has high natural reserves and is composed of diatoms skeletons or frustules and present abundantly in nature.[16] As a material, diatomite is a highly ordered porous structure composed of amorphous silica and exhibits high thermochemical stability, high surface area, low density, high absorption capacity, nontoxicity, excellent biocompatibility, and high adsorption properties.[16] Moreover, diatomite is a biomaterial with documented noncytotoxic properties that make it an effective delivery system with high ability to replace synthetic silica and address the bioavailability problem of water-insoluble drugs.[17−19] The functionalization of the diatomite structure by different chemical groups or integrating it in a composite was reported as an effective technique to induce its drug loading properties and drug release behavior.[17]

The functionalization of the silicate and silica porous structures was inspected as a promising modification technique that is valuable in enhancing their technical properties and performance as drug carriers.[10,20] The integration of biopolymers has a strong influence in enhancing the biocompatibility and biodegradability of the carrier as well as its affinity for the organic molecules of the drugs.[21,22] Chitosan is a highly recommended biopolymer in several medical applications and drug delivery systems. Chemically, it is known as a type of polyaminosaccharide and bioactive compound that exhibits promising biocompatibility, biodegradability, excellent loading capacity, low immunogenicity, low mucoadhesivity, and nontoxicity.[23,24] This supports the beneficial integration between chitosan and the various types of silica and silicate-based structure to produce a potential carrier with enhanced technical and pharmaceutical properties.

Therefore, this study aims to evaluate the suitability of diatomite as a natural and low-cost mesoporous silica to be used as an advanced delivery system for IB dug molecules instead of the expensive synthetic mesoporous silica. Additionally, this study involved facile functionalization of the diatomite structure with chitosan chains as a technique to enhance its technical and biocompatible properties as a drug carrier. The loading and the release properties were investigated for the first time in this study considering the essential factors. Additionally, the loading mechanism was addressed based on the equilibrium, kinetic, and thermodynamic studies. Moreover, the release behavior was discussed based on different release kinetic models.

2. RESULTS AND DISCUSSION

3.1. Characterization of the Carrier. *3.1.1. XRD Analysis.* XRD patterns were inspected to study the changes in the crystalline phases with the formation of CS/D composite (Figure 1). The observed broad diffraction peak at $2\theta = 22°$ is assigned to the amorphous silica of the characteristic diatomite opaline structure (Figure 1A). The diffraction peaks of chitosan were observed at $2\theta = 10$ and 22°, which indicate the semicrystalline properties of the commercial chitosan (Figure 1B). The XRD pattern of the CS/D composite clearly shows that the main peak of diatomite slightly deviated to $2\theta \sim 26°$ (Figure 1C). Additionally, one of the two significant peaks of chitosan disappeared and the other diffraction peak shifted and integrated with the fundamental peak of diatomite that assured the effective integration between diatomite precursor and chitosan biopolymer. The observed

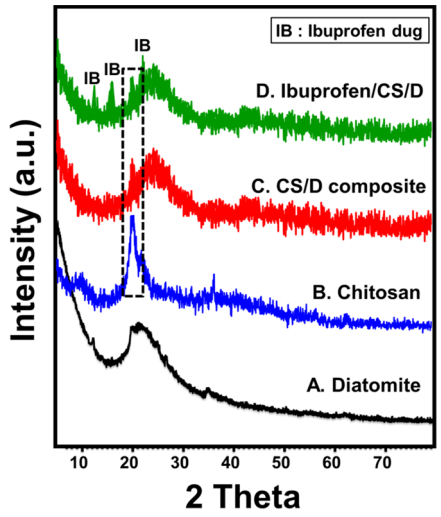

Figure 1. XRD patterns of raw diatomite (A), chitosan powder (B), prepared chitosan/diatomite composite (CS/D) (C), and ibuprofen-loaded CS/D composite (D).

pattern of the CS/D composite after loading it with the IB drug molecules revealed the presence of three reduced peaks related to the drug at 12.2, 16.65, and 22.31° (ICCD PDF2: 00-032-1723) (Figure 1D). Such a pattern strongly confirms the successful loading of the IB molecules into the CS/D composite as a carrier.

3.1.2. Morphological Features. The changes in the surface morphology with the formation of the CS/D composite were examined based on both the SEM and TEM images. Figure 2A shows the well-developed pinnate frustule of diatomite with its significant porous structure, where its pores distributed in a regular manner. The SEM images of CS/D showed observable changes in the surface features of the diatomite frustules (Figure 2B). The diatomite skeletons were clustered partially and sometimes completely with the chitosan chains giving nearly a spherical shape as the general form (Figure 2B). The high magnification of the chitosan clusters reveals its formation as nanofibers, which commonly identify the chitosan chains (Figure 2C,D).

The HRTEM images of the CS/D composite demonstrate the successful entrapping of the diatomite particles within the tabular chains of chitosan that show the nanoporous properties of the structure (Figure 2E,F). The intersection between the chitosan tabular grains resulted also in secondary nanopores, which give the enhanced surface area and pore size distribution properties of the general structure, which in turn have a strong impact in inducing the loading capacity of the CS/D composite (Figure 2E,F). Depending on the SEM and HRTEM images, the CS/D composite was formed with a particle size range of 100 nm to 50 μm considering the different sizes of the diatomite frustules.

Such changes in the morphologies are associated with noticeable changes in the textural properties. The surface area of diatomite enhanced obviously after the integration process from 117.7 m^2/g (DI) to 162.4 m^2/g (CS/D), and the pore diameter increased from 5.41 nm (DI) to 5.83 nm (CS/D). Such an enhancement can be explained as a result of the orientation of the diatomite frustules in the tabular shape of diatomite, the fibrous properties of the integrated chitosan, and the secondary pores that were formed by intersecting the chitosan chains with each other. Such results will have a strong

https://doi.org/10.1021/acsomega.1c01514
ACS Omega 2021, 6, 13406−13416

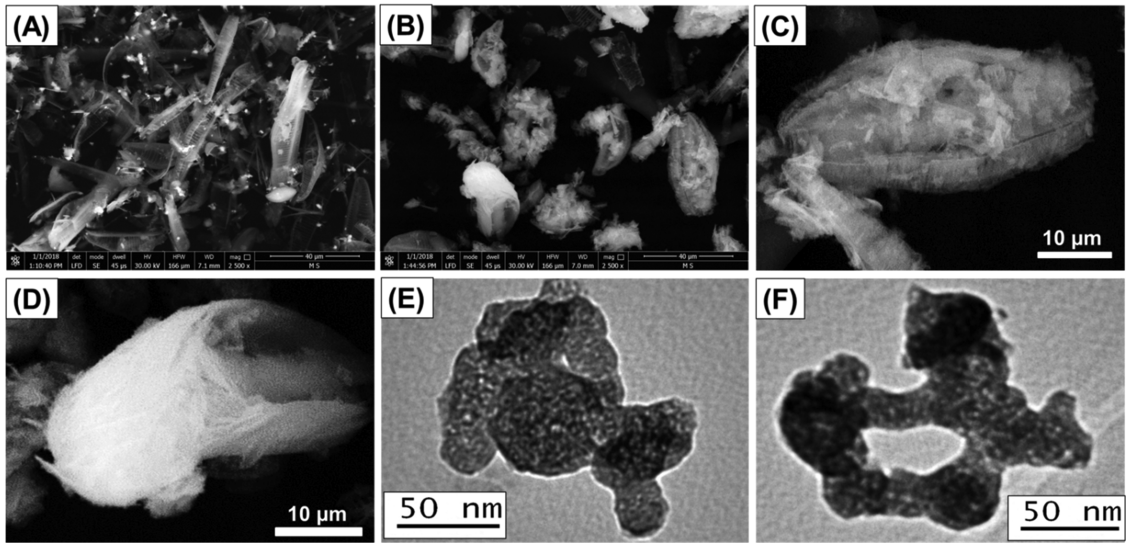

Figure 2. SEM image of diatomite precursor (A), synthetic CS/D composite (B), high-magnification image of the chitosan cluster on the surface of diatomite frustules (C), high-magnification image of the formation of chitosan as nanofibers (D), and TEM images of the CS/D composite reflecting enclosing of diatomite grains within the chitosan matrix (E, F).

influence in inducing the loading capacity of CS/D for IB drug molecules compared to the single phase of DI.

3.1.3. Fourier Transform Infrared (FT-IR) Analysis. The chemical structures of the produced CS/D composite, as well as its components, were investigated based on their FT-IR spectra as shown in Figure 3. The principal peaks of the refined

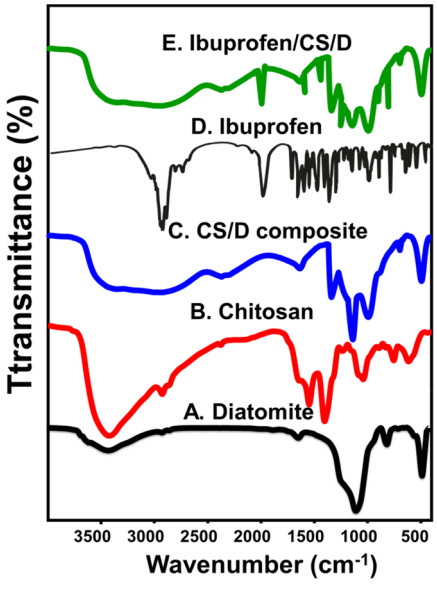

Figure 3. FT-IR spectra of diatomite (A), chitosan (B), chitosan/diatomite composite (CS/D) (C), ibuprofen drug (IB) (D), and IB-loaded CS/D composite (E).

diatomite material revealed two main bands at 3437 and 1638 cm^{-1}, which were corresponding to vibrations of silanol groups (Si−O−H) of the opaline silica structure and adsorbed water molecules (H−O−H) on the surface of diatomite (Figure 3A).[16] The other two bands were observed at 1092 and 799 cm^{-1}, which were related to the stretching of Si−O−Si in symmetric and asymmetric motions, respectively, in addition to Si−O vibration at 465 cm^{-1} (Figure 3A).[16] The major peaks of pure chitosan were observed at 3423 and 3423 cm^{-1} due to vibration modes of O−H and N−H, respectively[24] (Figure 3B). Besides, other absorption bands appeared at 2915, 1637, 1402, and 1040 cm^{-1}, which indicated the presence of all C−H, C═O, C−N, and C−O, respectively (Figure 3B).[24]

After the integration process, the spectrum of CS/D shows a significant increase in the intensities of the main peaks of amorphous silica at 3433 cm^{-1} compared to the observed bands for diatomite as a single phase (Figure 3C). Additionally, the other identification bands of diatomite were reported in the composite as Si−O and Si−O−Si groups at deviated positions (Figure 3C). The characteristic bands of chitosan were also detected in the composite and represented by C═O, C−N, and C−O, which were recognized by their deviated positions (Figure 3C). The results confirm the formation of composite from chitosan and diatomite. Additionally, the strong reduction or disappearance of the characteristic N−H groups of chitosan and the identification band of silanol groups in diatomite reflected the reactivity of both groups in forming a complex with each other as the suggested mechanism for the formation of the CS/D composite.

After the loading process, the obtained spectrum reflected the existence of some bands related to the chemical structure of the ibuprofen drug (Figure 3D,E). The identified bands are related to the carbonyl groups (1753 cm^{-1}), aromatic ring of IB molecules (700−1500 cm^{-1}), stretching of aromatic C═C (1421 cm^{-1}), and stretching of aromatic C−H (783 cm^{-1}) (Figure 3D,E).[25]

3.2. Loading Studies of Ibuprofen Drug. *3.2.1. Effect of the Loading Factors. 3.2.1.1. Effect of pH Values.* The pH values of the loading process have a critical impact on the loading capacity as they affected the properties of both the dissolved IB molecules and the surfaces of the carriers. The investigation of the influence of pH values on the IB loading capacity was performed within the pH range of 2−8, and the other loading experimental conditions were selected at pH 6, an IB concentration of 500 mg/L, a loading time of 4 h, a volume of 50 mL, and a temperature of 30 °C (Figure 4A). The resulted pH-dependent curves for both DI and CS/D demonstrate an obvious increase with pH increasing from pH 2 to 6 (Figure 4A). After that, the determined IB loading

https://doi.org/10.1021/acsomega.1c01514
ACS Omega 2021, 6, 13406−13416

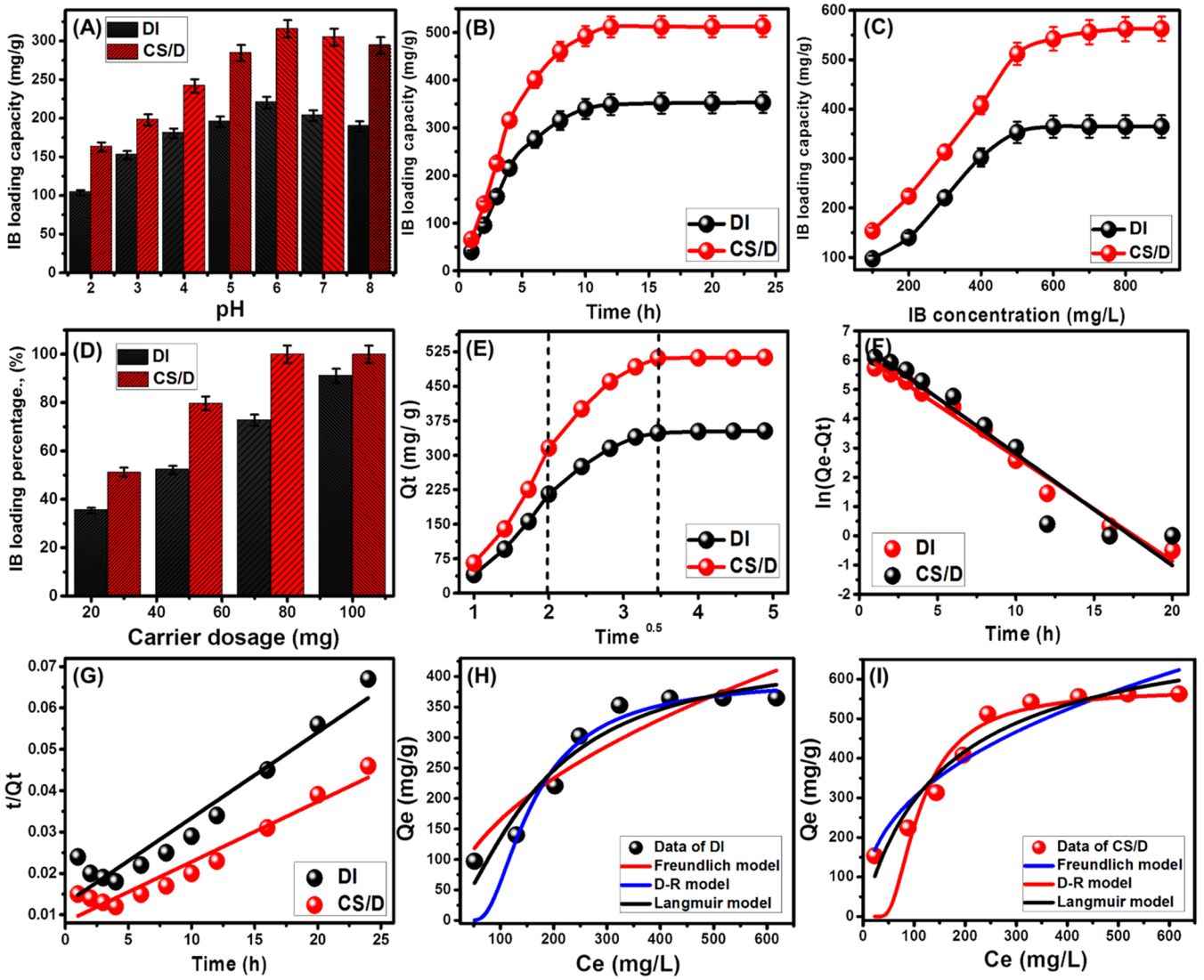

Figure 4. Influence of pH on the loading properties of IB into DI and CS/D (A); influence of contact on the loading properties of IB into DI and CS/D (B); influence of IB concentration on its loading properties into DI and CS/D (C); influence of the used dosage on the loading properties of IB into DI and CS/D (D); intraparticle diffusion curves for the loading of IB into DI and CS/D (E); fitting of the IB loading data with pseudo-first-order kinetic model (F); fitting of the IB loading data with pseudo-second-order kinetic model (G); fitting of the IB loading data by DI with the different isotherm models (H); and fitting of the IB loading data by CS/D with the different isotherm models (H).

capacities declined significantly up to pH 8. The poor IB loading capacities of DI and CS/D under the acidic conditions related to the reported hydrophobic properties of IB molecules under such conditions; therefore, it shows poor solubility and is present in molecular forms.[26] The systematic increase in the pH prompts the hydrophilic properties of the IB molecules and their solubility, which in turn facilitated the loading process, which can be observed up to pH 6. Above pH 6, the strong deprotonation properties of DI and CS/D carriers resulted in strong electrostatic repulsive properties between their negatively charged active sites and the carboxylate groups of the IB drug, which also have negative charges.[25,27] Therefore, the best pH for the effective loading of IB drug into DI and CS/D as drug carrier systems is pH 6 (Figure 4A). Additionally, the previous results show the strong influence of the integrated chitosan chains in inducing the affinity of siliceous diatomite for the organic IB molecule (Figure 4A). This enhanced the loading capacity of diatomite and showed a significant influence in controlling the loading capacities according to the required drug dosages based on the conditions of the loading process.

3.2.1.2. Effect of the Loading Interval. The influence of loading time on the loading capacities of the IB drug by DI and CS/D was followed from 1 to 24 h to select the equilibrium loading interval. The loading experimental conditions were selected at pH 6, an IB concentration of 500 mg/L, a carrier dosage of 25 mg, a volume of 50 mL, and a temperature of 30 °C (Figure 4B). The loading behaviors of IB as a function of the time interval by CS/D as well as DI demonstrate segments related to different loading rates. The first portions of these loading curves exhibit a strong increase in the measured loading capacities and very fast loading rates (Figure 4B). This is followed by portions of very limited increase in the IB loading capacities of DI and CS/D and nearly fixed rates, demonstrating stages of loading equilibrations (Figure 4B). This behavior can be explained according to the availability of the active loading sites as they are gradually occupied with the IB molecules until their complete filling in the drug.[28] This

https://doi.org/10.1021/acsomega.1c01514
ACS Omega 2021, 6, 13406−13416

shows the reported decrease in the loading rates with time as the number of the free loading sites occupy with increasing time. The tests revealed significant growth in the loaded quantities of the IB drug with an increase of loading time from 1 to 12 h for both diatomite (DI) and the CS/D composite (Figure 4B). After equilibration, the achieved IB equilibrium loading capacities of DI and CS/D are 353 and 512 mg/g, respectively. These values demonstrate the complete saturation of the carrier by the loading of IB drug molecules (Figure 4B).

3.2.1.3. Effect of Ibuprofen Concentration. Assessing the loading properties of DI and CS/D at different IB concentrations is of valuable impact to detect their maximum capacities as well as the equilibrium behaviors of the loading reactions. The IB concentration was studied from 100 to 900 mg/L, and the other loading experimental conditions were adjusted at certain values (pH 6; loading time, 24 h; carrier dosage, 25 mg; volume, 50 mL; temperature, 30 °C (Figure 4C)).

The IB loading capacities by DI and CS/D as carriers were induced strongly by conducting loading tests at high IB concentrations (Figure 4C). This behavior can be attributed to the influence of higher IB concentrations in accelerating the driving forces of its molecules, which has a strong influence in inducing the interaction chances with the active loading sites of the carriers.[10,29] Such enhancement in the IB loading quantities was reported with a certain range for the studied concentrations (from 100 to 500 mg/L for DI and from 100 up to 600 mg/L for CS/D) (Figure 4C). Beyond these concentrations, the determined loading capacities show limited increase or fixed values demonstrating the maximum capacities of the studied carriers (365 mg/g for DI and 562.6 mg/g for CS/D) (Figure 4C).

3.2.1.4. Effect of Dosages. The predicted control for the loaded percentages of IB drug at a certain concentration was studied as a function of the used dosages of the DI and CS/D as carriers from 25 to 100 mg. The loading experimental conditions were pH 6; IB concentration, 500 mg/L; loading time, 24 h; volume, 50 mL; and temperature, 30 °C. The loading percentages of IB enhanced strongly with the incorporation of the DI and CS/D carrier at high dosages (Figure 4D). The loading percentages of IB using DI enhanced by 35.3, 52.1, 72.7, and 91.2% with increasing dosage by 25, 50, 75, and 100 mg, respectively (Figure 4D). For CS/D carrier, the obtained loading percentages at its studied dosages of 25, 50, and 75 mg are 51.2, 79.7, and 100%, respectively (Figure 4D). Such a strong enhancement in the IB loading percentages as a function of the DI and CS/D dosages is related to the increase in the exposed active and free loading sites as well as the total surface area, which has a strong impact on enhancing the interaction properties with the dissolved ions.[30]

3.2.2. Loading Mechanism. 3.2.2.1. Kinetic Studies. The kinetic behaviors of the IB loading reactions into DI and CS/DI were described considering the signification of the intraparticle diffusion model in addition to both pseudo-first-order and pseudo-second-order models (Table S1). The intraparticle diffusion curves for IB loading processes into DI and CS/DI show three observable segments related to two different loading mechanisms in addition to the diffusion effect of the IB molecules (Figure 4E). The first identified segment related to the loading mechanism is controlled by the available free loading sites on the surfaces of the carriers[29] (Figure 4E). This was followed by the second segment related to the saturation of the surficial loading sites and the operation of the layered adsorption process as the effective loading mechanism[31] (Figure 4E). The detected segment after that is dominant during the equilibrium intervals, and the loading process affected interionic attraction and/or molecular association mechanisms.[32]

The fitting properties of IB loading reactions using DI showed a strong agreement with the pseudo-first-order model (PF), while the IB loading properties by the CS/D composite show higher agreement with the pseudo-second-order model, considering the values of both chi-squared (χ^2) and determination coefficient (R^2) (Figure 4F,G; Table 1).

Table 1. Theoretical Parameters of the Studied Kinetic and Isotherm Models in Addition to the Thermodynamic Parameters

model	parameters	DI	CS/D
pseudo-first-order	K_1 (min^{-1})	0.3557	0.3817
	$qe_{(cal)}$ (mg/g)	365.4	573
	R^2	0.98	0.91
	X^2	0.65	4.3
pseudo-second-order	k_2 (g mg^{-1} min^{-1})	3.4×10^{-4}	2.5×10^{-4}
	$qe_{(cal)}$ (mg/g)	386.5	523
	R^2	0.922	0.93
	X^2	1.54	2.8
Langmuir	q_{max} (mg/g)	440.39	765.5
	b (L/mg)	4.09×10^{-4}	0.0076
	R^2	0.93	0.91
	X^2	4.14	4.65
	R_L	0.75−0.92	0.141−0.396
Freundlich	$1/n$	0.5	0.39
	k_F (mg/g)	16.4	47.7
	R^2	0.87	0.88
	X^2	5.63	5.86
D−R model	β (mol^2/KJ^2)	0.0084	0.0079
	q_m (mg/g)	396	574.6
	R^2	0.86	0.84
	X^2	6.78	6.88
	E (KJ/mol)	7.71	7.95
ΔG° (kJ mol^{-1})	303.15	−22.51	−24.55
	308.15	−22.84	−24.77
	313.15	−22.98	−25.03
	318.15	−23.10	−25.23
	323.15	−23.28	−25.40
ΔH° (kJ mol^{-1})		−11.6	−11.46
ΔS° (J K^{-1} mol^{-1})		36.27	43.22

Therefore, the IB loading reactions by DI show more physical properties and those by CS/D show more chemical affinity. The reported good fitness with both models suggests the existence of some chemical process as complexation and hydrogen binding in addition to the strong effect of the electrostatic attractions as a physical process.[32,33]

3.2.2.2. Isotherm Studies. Langmuir and Freundlich models in addition to the Dubinin−Radushkevich (D−R) assumptions were applied to follow the loading equilibrium properties of IB using DI and CS/DI as carriers (Figure 4H,I; Table 1). Both χ^2 and R^2 were used to identify the fitting degrees, and their values reveal the IB loading properties according to the Langmuir isotherm behavior considering the recognized values for the Freundlich model. Therefore, the IB loading processes

https://doi.org/10.1021/acsomega.1c01514
ACS Omega 2021, 6, 13406−13416

show homogeneous behaviors and the loaded IB molecules exhibit monolayer form.[33,34] Moreover, the calculated RL parameter demonstrates values (<1) related to favorable loading reactions (Table 1). The maximum IB loading capacities of DI and CS/DI as theoretical values are 440.4 and 765.5 mg/g, respectively.

The D−R model has a strong influence in categorizing the types of the IB loading reactions based on the Gaussian energy (Figure 4H,I; Table 1).[33,34] The calculated values of Gaussian energy for DI and CS/DI are 7.71 and 7.95 kJ/mol, respectively. These values within the range of the physical reactions but estimating their values close to the range of the chemical process suggested complex physical and chemical mechanisms with dominant physical effects.[29]

3.2.2.3. Thermodynamic Properties. The thermodynamic behavior of DI and CS/D during the loading process of the IB drug was assessed within the temperature range of 30−50 °C. The loading experimental conditions were selected at pH 6; IB concentration, 500 mg/L; loading time, 4 h; and volume, 50 mL. The Gibbs free energy (ΔG°), as well as the enthalpy (ΔH°) and the entropy (ΔS°) were determined considering eq 1 and fitting the results with the van't Hof equation (eq 2), respectively (Figure 5; Table 1)[35]

$$\Delta G^\circ = -RT \ln K_c \quad (1)$$

$$\ln(K_c) = \frac{\Delta S^\circ}{R} - \frac{\Delta H^\circ}{RT} \quad (2)$$

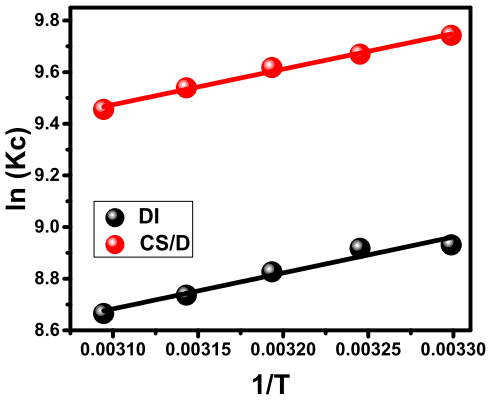

Figure 5. Fitting of the IB loading results by DI and CS/D with the van't Hof equation.

The ΔG° values that have negative signs for the loading process of the IB drug into DI and CS/D are related to favorable, feasible, and spontaneous chemical reactions (Table 1). The negative signs of the calculated enthalpies demonstrate the exothermic loading behavior for the IB drug into the DI and CS/D carriers (Table 1). The entropies were estimated as positive values, which signify the increase in the randomness of the reaction at high-temperature values (Table 1). The presented values of both ΔG° and ΔH° confirm the previous suggestion from the kinetic and equilibrium studies about the presence of complex mechanisms during the loading of IB related to both physical and chemical processes with more dominance for the physical effect.

3.2.2.4. Suggested Mechanism. The presented carrier is a hybrid structure from chitosan and diatomite, which represent multifunctional active groups of organic and inorganic nature. The loading of IB drug molecules in the diatomite substrate involved an electrostatic attraction mechanism in addition to the strong hydrogen bonding between the active silanol groups and the carboxylic groups of the drug.[10,36] For the integrated chitosan polymer, it also can achieve effective loading for the IB molecules by the electrostatic attractive forces between the chemical groups and the functional groups of the drug. Moreover, the IB molecules have the ability to form chemical complexes with the chitosan chains by the formation of hydrogen bonds between the IB carboxylic groups and the active groups of chitosan as the N−H groups and the OH-bearing groups[37] (Figure 3). This was supported by the recognized FT-IR spectrum of CS/D after the loading process as the characteristic bands of the silanol groups of diatomite and the identification bands of chitosan were reported at deviated positions and reduced intensities (Figure 3).

3.3. In Vitro Release Profiles. The IB release profiles of DI and CS/D as carriers within both the gastric fluid (pH 1.2) and the intestinal fluid (pH 7.4) show two segments or two different releasing rates (Figure 6). During the initial releasing intervals, the DI and CS/D carriers show fast IB release rates forming the first segments (Figure 6). After certain intervals, the two carriers exhibit very slow IB release rates or nearly fixed rates forming the second segment that is commonly recognized as the release equilibration stage (Figure 6). The first segment is related to the abrupt diffusion of IB molecules from the surficial active loading sites with the initiation of the release tests.[38] After that, the release behavior of the IB drug became limited by its entrapped molecules within the pores of the diatomite frustules and within the polymeric matrix of chitosan polymer.[12,39]

The IB release profile of diatomite (DI) as a separated phase reflects a very slow release behavior that continued up to 200 h without achieving the complete release for the loaded IB dosage either in the gastric or intestinal fluids (Figure 6). Such a slow and poor IB release profile for diatomite is related to the strong hydrogen bonding, which might be formed between diatomite by its silanol groups (Si−OH) and the IB drug by its carboxylate groups (COO−).[36] Under acidic conditions (gastric fluid (pH 1.2)), about 50% of the loaded IB quantity was released after 60 h and 73.4% was released after 180 h, which is the maximum release value of IB from diatomite (Figure 6A). Under basic conditions (intestinal fluid (pH 7.4)), the observed IB release percentages increased greatly to achieve diffusion for 50 and 87.4% of the loaded IB quantity after 40 and 140 h, respectively (Figure 6B). Then, the release percentage was fixed at this value (87.4%) up to 200 h, i.e., the maximum release percentage (Figure 6B). The observed increase in the release rates and the release percentages of IB drug in the intestinal fluid (pH 7.4) were related to its high solubility properties under alkaline conditions compared to acidic environments.[40] The IB drug as adsorbed molecules within the pores of diatomite is of ionic state, and performing the release tests at a high pH (pH > 7) induces the solubility and the diffusion of such ions to the buffer solutions. Conducting the tests at a low pH (acidic conditions) prompted the existence of the IB drug in its molecular form, which causes the accumulation of the drug molecules within the structural pores of diatomite and reduces its diffusion efficiency during the release tests.[10,40]

The integration of diatomite and chitosan in a composite (CS/D) results in an obvious increase in the IB release rates with more controlled properties. Conducting the release test within the gastric fluid (pH 1.2) resulted in release percentages

https://doi.org/10.1021/acsomega.1c01514
ACS Omega 2021, 6, 13406−13416

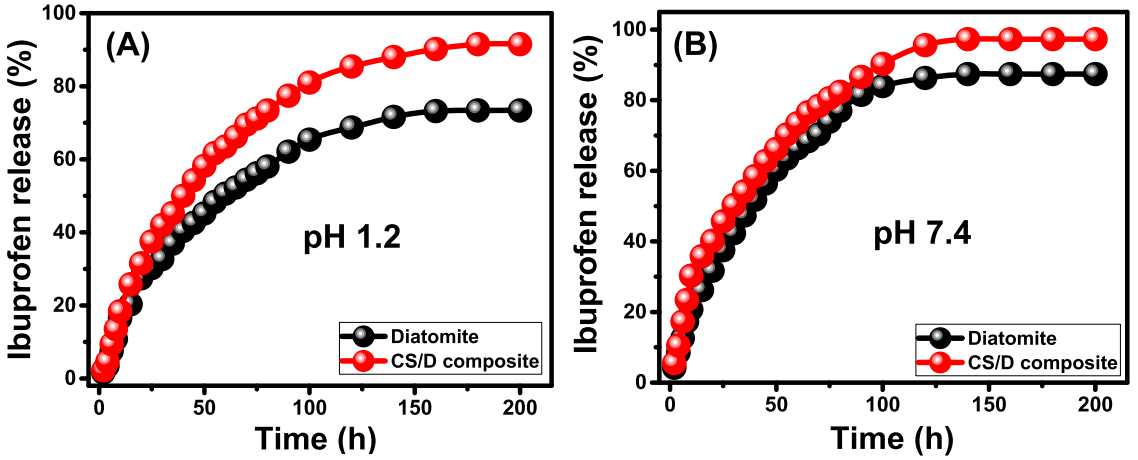

Figure 6. In vitro IB release profiles from DI and CS/D composite as carriers at the gastric fluid (pH 1.2) (A) and the intestinal fluid (pH 7.4) (B).

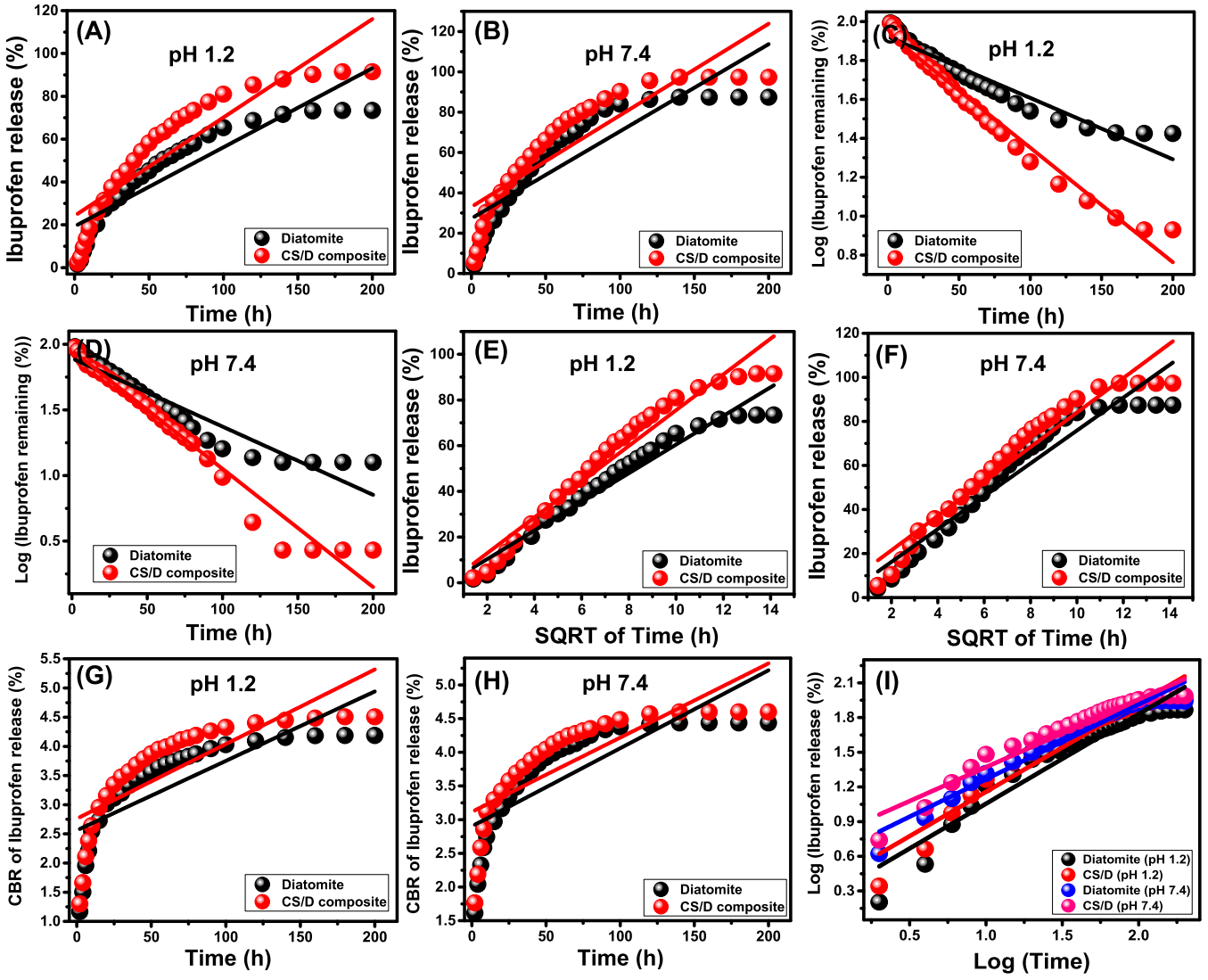

Figure 7. Fitting of the IB release results from both DI and CS/D with zeroth-order model (A, B), first-order model (C, D), Higuchi model (E, F), Hixson–Crowell model (G, H), and Korsmeyer–Peppas (I)

of 50 and 91.5% after 40 and 180 h, respectively (Figure 6A). The maximum IB release percentage is 91.5%, and this value is fixed from 180 to 200 h without achieving the complete release (100%) of the loaded IB quantity (Figure 6A). Within the intestinal fluid (pH 7.4), the CS/D composite as a carrier for IB drug exhibits release profiles of 50 and 95% IB release percentages after 30 and 120 h, respectively (Figure 6B). The detected maximum IB release percentage at this pH (pH 7.4)

https://doi.org/10.1021/acsomega.1c01514
ACS Omega 2021, 6, 13406−13416

is 97.3%, which was detected at fixed values from 140 to 200 h (Figure 6B). The reported high IB release properties of the CS/D composite at pH 7.4 (intestinal fluid) were assigned to the high solubility of the drug at the basic environments rather than the acidic environment and the chitosan properties. The structural amino groups of chitosan have high protonation properties in acidic environments, which induce the formation of strong electrostatic attractive forces between them and the negatively charged carboxylate groups of the IB molecules, which reduce their diffusion into the buffer solution.[40] Moreover, the protonation process causes the formation of a hydrated layer on the surface of the CS/D composite, which has a negative influence on the IB molecules from the pores of the diatomite frustule or the polymeric matrix of chitosan.[41]

The faster IB release profile of the CS/D composite than the profile of diatomite as a separated phase is essentially related to the integrated chitosan chains. The polymeric matrix of chitosan acts as a barrier or a hindering surface between the active silanol groups of diatomite and the carboxylate groups of IB drug. This hinders the strong hydrogen bonding between them, which in turn accelerates the diffusion of the IB molecules. Moreover, the homogeneous entrapping of the loaded IB molecules within the polymeric matrix of the integrated chitosan has a significant effect in inducing their diffusion rates into the buffer solutions.[42]

Developing drug carriers or delivery systems of fast release profiles has a valuable effect for rapidly delivering the drugs to the body at the required therapeutic dosages in short time intervals. On the other hand, the systems that show slow and continuous release profiles have valuable influence in preserving the delivered drugs to the human body at their best therapeutic dosages for long periods.[7,41] Therefore, the developed CS/D composite has promising technical properties as a delivery system for the IB drug. It is of significant loading capacity that can be controlled according to the required dosages by adjusting the affected loading conditions. Additionally, it shows a controlled release profile in which the IB release percentage can be adjusted based on the ratio of the integrated chitosan to the diatomite substrate.

Comparing the obtained findings, the raw diatomite achieved a loading capacity of 440.4 mg/g, which is higher than the determined value for the synthetic mesoporous silica MCM-48 (343 mg/g). Also, the release profile of diatomite demonstrates the maximum IB release percentages of 73.4% (pH 1.2) and 87.4% (pH 7.4) for 180 and 140 h, respectively. The obtained IB release profile of MCM-48 resulted in release percentages of 79% (pH 1.2) and 91% (pH 7.4) after 200 h and 100 h, respectively.[10] Such results demonstrate the higher loading capacity of natural diatomite as mesoporous silica compared to the synthetic forms. Additionally, it shows a lower release rate compared to the synthetic mesoporous silica MCM-48.[10] And this behavior obviously enhanced after its integration with chitosan and results in a compatible carrier of high loading properties and controlled release behavior.

3.4. Release Kinetics. The kinetic properties of DI and CS/D during the release of the loaded IB molecules were assessed based on the theoretical assumptions of several kinetic models including the zeroth-order model (Figure 7A,B), the first-order model (Figure 7C,D), the Higuchi model (Figure 7E,F), the Hixson−Crowell model (Figure 7G,H), and the Korsmeyer−Peppas model (Figure 7I,J). The fitting degrees were determined based on the values of the determination coefficient (R^2), which were obtained from the linear regression fitting processes considering the linear equations of the model as eqs 3−7 in order.[12]

$$W_t - W_0 = K_0 \cdot t \tag{3}$$

$$\ln(W_\infty / W_t) = K_1 \cdot t \tag{4}$$

$$W_t = K_h t^{1/2} \tag{5}$$

$$W_o^{1/3} - W_t^{1/3} = K_{HC} t \tag{6}$$

$$W_t / W_\infty = K_p\, t^n \tag{7}$$

The zeroth-order model as a kinetic release model suggests the possible release of the IB molecules from the DI and CS/D carriers at fixed rates at all of the studied intervals of the release process without a significant influence on the concentration of IB as loaded molecules.[43] On the other hand, the release behaviors that followed the first-order model involved a significant effect for the IB concentration as a loaded drug during the release process.[39] The Higuchi model as a kinetic model can be used to illustrate the release processes in which the diffusion of the loaded IB drug molecules is the essential release mechanism.[39] During the release process, six assumptions are possible, showing Higuchi behavior: (1) the IB concentration of loaded molecules is higher than their dissolving rates, (2) the diffusion behavior of IB molecules will be controlled in one direction, (3) the size of IB as loaded molecules is smaller than the actual thickness of their carriers, (4) the solubility and swelling behavior of the polymeric components have a negligible effect during the release process, (5) the used carriers show fixed diffusion rates for the loaded molecules, and (6) the release process reflects the strong sink properties for the loaded IB drugs.[43,44]

The Hixson−Crowell model as the release kinetic model suggests a dominant influence for the erosion mechanism during the release processes. Additionally, according to this model, the release of IB as a loaded drug occurs in parallel planes, and the release efficiency depends strongly on the surface area and the grain diameter of the DI and CS/D as carriers.[7] The Korsmeyer−Peppas model is a vital kinetic model and has strong significance during the illustration of the release mechanisms of the loaded drugs from delivery systems, which contain polymeric components.[39]

The values of the determination coefficient (R^2), which were obtained from the linear regression fitting of the release results from DI and the CS/D composite with the kinetic models, are presented in Table 2. Based on the values, the release of IB from both DI and CS/D follows first-order model behavior rather than the assumption of the zeroth-order model. Therefore, the concentration of IB as loaded molecules has a strong influence in controlling the release profiles from DI and CS/D as carriers. Regarding the Higuchi model, the IB release results from DI and CS/D also have good agreement with its release properties, suggesting the diffusion of the IB molecules from the structural pores of diatomite as well as the polymeric matrix of chitosan. The R^2 values demonstrate the poor agreement between the IB release results from both DI and CS/D and the assumption of the Hixson−Crowell model.

Finally, the R^2 values show that the best fitting degree was obtained for the Korsmeyer−Peppas model. The diffusion exponent (n) values, which were calculated as a theoretical parameter for the model (0.77 (pH 1.2) and 0.65 (pH 7.4) for DI; and 0.76 (pH 1.2) and 0.86 (pH 7.4) for CS/D) are within

https://doi.org/10.1021/acsomega.1c01514
ACS Omega 2021, 6, 13406−13416

Table 2. Determination Coefficient Values for the Fitting Process of the Release Results with the Different Kinetic Models

		determination coefficient (R^2)	
models	materials	pH 1.2	pH 7.4
zeroth-order model	DI	0.80	0.79
	CS/D	0.75	0.76
first-order model	DI	0.92	0.89
	CS/D	0.97	0.96
Higuchi model	DI	0.92	0.92
	CS/D	0.93	0.93
Hixson−Crowell model	DI	0.60	0.61
	CS/D	0.60	0.60
Korsmeyer−Peppas model	DI	0.94	0.95
	CS/D	0.94	0.94

the suggested levels for the non-Fickian transport release reactions (anomalous release). Such a release behavior is related to the operation of both erosion and diffusion processes during the release of the IB molecules from DI and CS/D carriers.[7] Considering the recognized fitting results with Higuchi, Hixson−Crowell, and Korsmeyer−Peppas models, the release of IB from the CS/D composite involves erosion and diffusion processes, but with an essential or dominant role for the diffusion process compared to the effect of the erosion process.

4. CONCLUSIONS

Chitosan/diatomite nanocomposite (CS/D) was synthesized as a low-cost and advanced carrier for ibuprofen drug (IB). The CS/D composite has a promising IB loading capacity (562.6 mg/g), which is higher than DI (365 mg/g). The IB loading process can be described according to the pseudo-second-order kinetic and Langmuir isotherm behaviors. The IB loading processes occur in monolayer form and show homogeneous properties involving mainly physical reactions. The thermodynamic studies demonstrate spontaneous, favorable, and exothermic IB loading reactions. The synthetic CS/D carrier is of significant IB release profile for about 200 h with maximum releases of 91.5 and 97.3% at the gastric fluid (pH 1.2) and intestinal fluid (pH 7.4), respectively. The IB release mechanism involved diffusion and erosion processes considering the estimated value of diffusion exponent as a parameter from the Korsmeyer−Peppas kinetic model.

5. EXPERIMENTAL WORK

5.1. Materials. The chemical composition of the purified diatomite precursor was SiO_2 (97.87%), Al_2O_3 (1.79%), and L.O.I (0.34%); it was obtained from Central Metallurgical and Development Institute, Egypt. Hydrochloric acid (37% purity) and hydrogen peroxide (30% purity) were used in the leaching process of the diatomite sample and obtained from Cornel Lab Company, Egypt. Chitosan (CS) polymer powder of deacetylation degree (MW 120 000; 85%) and acetic acid (99.8%) were used in the synthesis of the composite with diatomite and were delivered from Sigma-Aldrich, Egypt. Ibuprofen drug of analytical grade (98%) was obtained from Sigma-Aldrich to perform the loading and release experiments.

5.2. Preparation of Chitosan/Diatomite Carrier (CS/D). The natural diatomite precursor (5 g) was impregnated into HCl (10%) at 100 °C for 4 h under stirring to remove the metallic impurities. Then, the purified sample was treated with H_2O_2 three times to leach the present impurities that are of organic nature. Finally, the refined diatomite was washed with distilled water and oven-dried at 80 °C for 12 h for the further synthesis steps. After that, 3 g of the purified diatomite precursor was immersed in 50 mL of distilled water under sonication (240 W) for 120 min to ensure the homogeneous dispersion for its particles. Then, the mixture was impregnated homogeneously within the chitosan gel, which was obtained by soaking 3 g of chitosan biopolymer in 50 mL of acetic acid solution (0.1 M) under sonication (240 W) and magnetic stirring (800 rpm) for 12 h. The produced CS/D carrier was filtrated and washed well to remove excess amounts of acetic acid. As the final step, the CS/D composite was dried overnight at 60 °C and labeled as CS/D for further characterization, loading, and release studies.

5.3. Characterization Techniques. The crystalline changes of the diatomite/chitosan composite before and after the loading process with ibuprofen drug as well as the individual components were followed by XRD diffraction (PANalytical (Empyrean)). The diffractometer is of Cu Kα radiation, and the pattern of the materials was estimated within 2θ range of 5−70° at 5°/min scanning speed and 40 kV operating voltage. The differences between the functional groups of the loaded and unloaded composites as well as the integrated components were inspected by an FT-IR spectrometer (Bruker, Vertex 70). The determination was conducted with a frequency range of 400−4000 cm^{-1}. The morphology, surface modifications, and internal features after the combination between chitosan and diatomite were analyzed by a scanning electron microscope (Gemini, Zeiss-Ultra 55) and a transmission electron microscope (JEOL-JEM2100). The specific surface area and the distribution of pore size of the CS/D composites were measured by a surface area analyzer (Beckman Coulter SA3100) after a degassing step at 30 °C for 5 h based on the BET and BJH data analysis methods, respectively.

5.4. Loading and Release Tests. *5.4.1. Loading Studies.* The loading properties of the CS/D composite as a carrier for ibuprofen drug (IB) were investigated considering various experimental parameters such as the influence of the IB concentration from 100 to 900 mg/L, CS/D dosages from 25 to 125 mg, time from 1 to 24 h, pH from 2 to 8, and temperature from 30 to 60 °C.[10] After each test, the loaded CS/D composite was separated by filtration and the remaining concentrations of IB were measured using a UV−vis spectrophotometer after adjusting its wavelength at the maximum absorbance wavelength of the IB drug (λ = 222 nm). Each loading test was repeated three times, and the calculated results were presented in their average values with a standard deviation of less than 5.3%. The quantities of the loaded IB drug into the CS/D carrier were calculated according to eq 8.

$$\text{Loaded drug(mg/g)} = \frac{(\text{Initial concentration} - \text{Residual concentration}) \times \text{solvent volume}}{\text{Carrier weight}} \quad (8)$$

5.4.2. In Vitro Release Studies. The in vitro release profile of CS/D composite was assessed using two buffer solutions of different pHs (intestinal fluid (pH 7.4) and gastric fluid (pH 1.2)).[10] The release tests were conducted by dispersing a certain quantity of IB-loaded CS/D (100 mg) within 500 mL

https://doi.org/10.1021/acsomega.1c01514
ACS Omega 2021, 6, 13406−13416

of the buffer solution, where the temperature was adjusted to be 37.5 °C for 200 h. The homogenization between the carrier and the solutions was performed utilizing a dissolution apparatus (DISTEK type, 4300), after which the vessels were rotated at a certain speed of 200 rpm. After that, regular samples from the buffer solutions (5 mL) during the release study were obtained and the diffused IB in the solutions was determined using a UV−vis spectrophotometer after adjusting its wavelength at the maximum absorbance wavelength of the IB drug (λ = 222 nm). After the measurements, the extracted samples were returned again to the bulk buffer solutions. Additionally, the release tests were conducted as triplicate tests and the reported release percentages are average values with a standard deviation of less than 4%. The release percentages of the loaded IB drug into CS/D were calculated based on eq 9.

$$\text{Drug release}(\%) = \frac{\text{The amount of Released LVX}}{\text{Amount of loaded LVX}} \times 100 \quad (9)$$

■ ASSOCIATED CONTENT

Supporting Information

The Supporting Information is available free of charge at https://pubs.acs.org/doi/10.1021/acsomega.1c01514.

Theoretical equations of the kinetic and isotherm models (Table S1) (PDF)

■ AUTHOR INFORMATION

Corresponding Author

Mostafa R. Abukhadra − *Materials Technologies and their Applications Lab, Geology Department, Faculty of Science, Beni-Suef University, Beni-Suef City 65211, Egypt; Geology Department, Faculty of Science, Beni-Suef University, Beni-Suef City 65211, Egypt;* orcid.org/0000-0001-5404-7996; Email: abukhadra89@science.bsu.edu.eg

Authors

Sherouk M. Ibrahim − *Materials Technologies and their Applications Lab, Geology Department, Faculty of Science, Beni-Suef University, Beni-Suef City 65211, Egypt; Chemistry Department, Faculty of Science, Beni-Suef University, Beni-Suef City 65211, Egypt*

May N. Bin Jumah − *Biology Department, Faculty of Science, Princess Nourah bint Abdulrahman University, Riyadh 11564, Saudi Arabia*

Sarah I. Othman − *Biology Department, Faculty of Science, Princess Nourah bint Abdulrahman University, Riyadh 11564, Saudi Arabia*

Reem Saleh Alruhaimi − *Biology Department, Faculty of Science, Princess Nourah bint Abdulrahman University, Riyadh 11564, Saudi Arabia*

Nora Al-Khalawi − *Biology Department, Faculty of Science, Princess Nourah bint Abdulrahman University, Riyadh 11564, Saudi Arabia*

Yasser F. Salama − *Geology Department, Faculty of Science, Beni-Suef University, Beni-Suef City 65211, Egypt*

Ahmed A. Allam − *Department of Zoology, Faculty of Science, Beni-Suef University, Beni-Suef City 65211, Egypt*

Complete contact information is available at: https://pubs.acs.org/10.1021/acsomega.1c01514

Author Contributions

This article was written through the contributions of all authors. All authors have given approval to the final version of the manuscript

Notes

The authors declare no competing financial interest.

Further studies will be conducted to investigate the properties of the Ibuprofen-loaded chitosan/diatomite composite in an in vivo study focusing on the hydrodynamic size of the carrier as well as its thermal properties. Additionally, the product will be investigated in several formulations considering different ratios for the integrated chitosan and the preparation pH.

■ ACKNOWLEDGMENTS

The authors thank the Deanship of Scientific Research at Princess Nourah bint Abdulrahman University for funding this work through the Research Groups Program grant no. (RG-1442-0035).

■ REFERENCES

(1) Macedo, L. D. O.; Barbosa, E. J.; Löbenberg, R.; Bou-Chacra, N. A. Anti-inflammatory drug nanocrystals: state of art and regulatory perspective. *Eur. J. Pharm. Sci.* **2020**, *158*, No. 105654.

(2) Chen, Q.; Di, L.; Zhang, Y.; Li, N. Chemical constituents with cytotoxic and anti-inflammatory activity in Hypericum sampsonii and the antitumor potential under the view of cancer-related inflammation. *J. Ethnopharmacol.* **2020**, *259*, No. 112948.

(3) Mahgoub, S. M.; Shehata, M. R.; El-Ela, F. L. A.; Farghali, A.; Zaher, A.; Mahmoud, R. K. Sustainable waste management and recycling of Zn−Al layered double hydroxide after adsorption of levofloxacin as a safe anti-inflammatory nanomaterial. *RSC Adv.* **2020**, *10*, 27633−27651.

(4) Tsivkovskii, R.; Sabet, M.; Tarazi, Z.; Griffith, D. C.; Lomovskaya, O.; Dudley, M. N. Levofloxacin reduces inflammatory cytokine levels in human bronchial epithelia cells: implications for aerosol MP-376 (levofloxacin solutionfor inhalation) treatment of chronic pulmonary infections. *FEMS Immunol. Med. Microbiol.* **2011**, *61*, 141−146.

(5) Wang, Y.; Ke, J.; Gou, K.; Guo, Y.; Xu, X.; Li, S.; Li, H. Amino functionalized mesoporous silica with twisted rod-like shapes: Synthetic design, in vitro and in vivo evaluation for ibuprofen delivery. *Microporous Mesoporous Mater.* **2020**, *294*, No. 109896.

(6) Javanbakht, S.; Nezhad-Mokhtari, P.; Shaabani, A.; Arsalani, N.; Ghorbani, M. Incorporating Cu-based metal-organic framework/drug nanohybrids into gelatin microsphere for ibuprofen oral delivery. *Mater. Sci. Eng., C* **2019**, *96*, 302−309.

(7) Abukhadra, M. R.; Refay, N. M.; El-Sherbeeny, A. M.; Mostafa, A. M.; Elmeligy, M. A. Facile synthesis of bentonite/biopolymer composites as low-cost carriers for 5-fluorouracil drug; equilibrium studies and pharmacokinetic behavior. *Int. J. Biol. Macromol.* **2019**, *141*, 721−731.

(8) Lu, C.; Xiao, Y.; Liu, Y.; Sun, F.; Qiu, Y.; Mu, H.; Duan, J. Hyaluronic acid-based levofloxacin nanomicelles for nitric oxide-triggered drug delivery to treat bacterial infections. *Carbohydr. Polym.* **2020**, *229*, No. 115479.

(9) Kuang, Z.; Dai, G.; Wan, R.; Zhang, D.; Zhao, C.; Chen, C.; Li, J.; Gu, H.; Huang, W. Osteogenic and antibacterial dual functions of a novel levofloxacin loaded mesoporous silica microspheres/nano-hydroxyapatite/polyurethane composite scaffold. *Genes Dis.* **2019**, *8*, 193−202.

(10) Abukhadra, M. R.; Refay, N. M.; El-Sherbeeny, A. M.; El-Meligy, M. A. Insight into the Loading and Release Properties of MCM-48/Biopolymer Composites as Carriers for 5-Fluorouracil: Equilibrium Modeling and Pharmacokinetic Studies. *ACS Omega* **2020**, *5*, 11745−11755.

(11) Safi, S.; Karimzadeh, F.; Labbaf, S. Mesoporous and hollow hydroxyapatite nanostructured particles as a drug delivery vehicle for the local release of ibuprofen. *Mater. Sci. Eng., C* **2018**, *92*, 712−719.
(12) Tian, L.; Abukhadra, M. R.; Mohamed, A. S.; Nadeem, A.; Ahmad, S. F.; Ibrahim, K. E. Insight into the Loading and Release Properties of an Exfoliated Kaolinite/Cellulose Fiber (EXK/CF) Composite as a Carrier for Oxaliplatin Drug: Cytotoxicity and Release Kinetics. *ACS Omega* **2020**, *5*, 19165−19173.
(13) Pajchel, L.; Kolodziejski, W. Synthesis and characterization of MCM-48/hydroxyapatite composites for drug delivery: Ibuprofen incorporation, location and release studies. *Mater. Sci. Eng., C* **2018**, *91*, 734−742.
(14) Rehman, F.; Ahmed, K.; Rahim, A.; Muhammad, N.; Tariq, S.; Azhar, U.; Khan, A. J.; Sama, Z. us.; Volpe, P. L.; Airoldi, C. Organo-bridged silsesquioxane incorporated mesoporous silica as a carrier for the controlled delivery of ibuprofen and fluorouracil. *J. Mol. Liq.* **2018**, *258*, 319−326.
(15) Amirsoleimani, M.; Khalilzadeh, M. A.; Zareyee, D. Preparation and catalytic evaluation of a palladium catalyst deposited over modified clinoptilolite (Pd@ MCP) for chemoselective N-formylation and N-acylation of amines. *J. Mol. Struct.* **2021**, *1225*, No. 129076.
(16) Liu, G.; Abukhadra, M. R.; El-Sherbeeny, A. M.; Mostafa, A. M.; Elmeligy, M. A. Insight into the photocatalytic properties of diatomite@ Ni/NiO composite for effective photo-degradation of malachite green dye and photo-reduction of Cr (VI) under visible light. *J. Environ. Manage.* **2020**, *254*, No. 109799.
(17) Janićijević, J.; Krajišnik, D.; Čalija, B.; Vasiljević, B. N.; Dobričić, V.; Daković, A.; Antonijević, M. D.; Milić, J. Modified local diatomite as potential functional drug carrier—A model study for diclofenac sodium. *Int. J. Pharm.* **2015**, *496*, 466−474.
(18) Bariana, M.; Aw, M. S.; Kurkuri, M.; Losic, D. Tuning drug loading and release properties of diatom silica microparticles by surface modifications. *Int. J. Pharm.* **2013**, *443*, 230−241.
(19) Rea, I.; Martucci, N. M.; De Stefano, L.; Ruggiero, I.; Terracciano, M.; Dardano, P.; Migliaccio, N.; Arcari, P.; Taté, R.; Rendina, I.; Lamberti, A. Diatomite biosilica nanocarriers for siRNA transport inside cancer cells. *Biochim. Biophys. Acta, Gen. Subj.* **2014**, *1840*, 3393−3403.
(20) Khalilzadeh, M. A.; Sadeghifar, H.; Venditti, R. Natural clinoptilolite/KOH: an efficient heterogeneous catalyst for carboxymethylation of hemicellulose. *Ind. Eng. Chem. Res.* **2019**, *58*, 11680−11688.
(21) Khalilzadeh, M. A.; Hosseini, S.; Rad, A. S.; Venditti, R. A. Synthesis of Grafted Nanofibrillated Cellulose-Based Hydrogel and Study of Its Thermodynamic, Kinetic, and Electronic Properties. *J. Agric. Food Chem.* **2020**, *68*, 8710−8719.
(22) Servatan, M.; Zarrintaj, P.; Mahmodi, G.; Kim, S. J.; Ganjali, M. R.; Saeb, M. R.; Mozafari, M. Zeolites in drug delivery: Progress, challenges and opportunities. *Drug Discovery Today* **2020**, *25*, 642−656.
(23) Shariatinia, Z. Pharmaceutical applications of chitosan. *Adv. Colloid Interface Sci.* **2019**, *263*, 131−194.
(24) Saad, A. M.; Abukhadra, M. R.; Ahmed, S. A. K.; Elzanaty, A. M.; Mady, A. H.; Betiha, M. A.; Shim, J. J.; Rabie, A. M. Photocatalytic degradation of malachite green dye using chitosan supported ZnO and Ce−ZnO nano-flowers under visible light. *J. Environ. Manage.* **2020**, *258*, No. 110043.
(25) Sogias, I. A.; Williams, A. C.; Khutoryanskiy, V. V. Chitosan-based mucoadhesive tablets for oral delivery of ibuprofen. *Int. J. Pharm.* **2012**, *436*, 602−610.
(26) Gao, L.; Sun, J.; Zhang, L.; Wang, J.; Ren, B. Influence of different structured channels of mesoporous silicate on the controlled ibuprofen delivery. *Mater. Chem. Phys.* **2012**, *135*, 786−797.
(27) Mostafa, M.; El-Meligy, M. A.; Sharaf, M.; Soliman, A. T.; AbuKhadra, M. R. Insight into chitosan/zeolite-A nanocomposite as an advanced carrier for levofloxacin and its anti-inflammatory properties; loading, release, and anti-inflammatory studies. *Int. J. Biol. Macromol.* **2021**, *179*, 206−216.
(28) Albukhari, S. M.; Salam, M. A.; Abukhadra, M. R. Effective retention of inorganic Selenium ions (Se (VI) and Se (IV)) using novel sodalite structures from muscovite; characterization and mechanism. *J. Taiwan Inst. Chem. Eng.* **2021**, *120*, 116−126.
(29) Salam, M. A.; Abukhadra, M. R.; Mostafa, M. Effective decontamination of As (V), Hg (II), and U (VI) toxic ions from water using novel muscovite/zeolite aluminosilicate composite: adsorption behavior and mechanism. *Environ. Sci. Pollut. Res.* **2020**, *27*, 13247−13260.
(30) Abukhadra, M. R.; Mohamed, A. S. Adsorption removal of safranin dye contaminants from water using various types of natural zeolite. *Silicon* **2019**, *11*, 1635−1647.
(31) Huang, Y.; Li, S.; Chen, J.; Zhang, X.; Chen, Y. Adsorption of Pb (II) on mesoporous activated carbons fabricated from water hyacinth using H3PO4 activation: adsorption capacity, kinetic and isotherm studies. *Appl. Surf. Sci.* **2014**, *293*, 160−168.
(32) Li, X.; Zhang, D.; Sheng, F.; Qing, H. Adsorption characteristics of Copper (II), Zinc (II) and Mercury (II) by four kinds of immobilized fungi residues. *Ecotoxicol. Environ. Saf.* **2018**, *147*, 357−366.
(33) Dinu, M. V.; Lazar, M. M.; Dragan, E. S. Dual ionic cross-linked alginate/clinoptilolite composite microbeads with improved stability and enhanced sorption properties for methylene blue. *React. Funct. Polym.* **2017**, *116*, 31−40.
(34) Dragan, E. S.; Dinu, M. V. Spectacular selectivity in the capture of methyl orange by composite anion exchangers with the organic part hosted by DAISOGEL microspheres. *ACS Appl. Mater. Interfaces* **2018**, *10*, 20499−20511.
(35) Tran, H. N.; You, S. J.; Hosseini-Bandegharaei, A.; Chao, H. P. Mistakes and inconsistencies regarding adsorption of contaminants from aqueous solutions: a critical review. *Water Res.* **2017**, *120*, 88−116.
(36) Kamarudin, N. H. N.; Jalil, A. A.; Triwahyono, S.; Salleh, N. F. M.; Karim, A. H.; Mukti, R. R.; Hameed, B. H.; Ahmad, A. Role of 3-aminopropyltriethoxysilane in the preparation of mesoporous silica nanoparticles for ibuprofen delivery: effect on physicochemical properties. *Microporous Mesoporous Mater.* **2013**, *180*, 235−241.
(37) Vieira, A. P.; Badshah, S.; Airoldi, C. Ibuprofen-loaded chitosan and chemically modified chitosans-Release features from tablet and film form. *Int. J. Biol. Macromol.* **2013**, *52*, 107−115.
(38) Tan, D.; Yuan, P.; Dong, F.; He, H.; Sun, S.; Liu, Z. Selective loading of 5-fluorouracil in the interlayer space of methoxy-modified kaolinite for controlled release. *Appl. Clay Sci.* **2018**, *159*, 102−106.
(39) El-Zeiny, H. M.; Abukhadra, M. R.; Sayed, O. M.; Osman, A. H.; Ahmed, S. A. Insight into novel *β*-cyclodextrin-grafted-poly (N-vinylcaprolactam) nanogel structures as advanced carriers for 5-fluorouracil: Equilibrium behavior and pharmacokinetic modeling. *Colloids Surf., A* **2020**, *586*, No. 124197.
(40) Goscianska, J.; Olejnik, A.; Nowak, I.; Marciniak, M.; Pietrzak, R. Ordered mesoporous silica modified with lanthanum for ibuprofen loading and release behavior. *Eur. J. Pharm. Biopharm.* **2015**, *94*, 550−558.
(41) Sun, L.; Chen, Y.; Zhou, Y.; Guo, D.; Fan, Y.; Guo, F.; Zheng, Y.; Chen, W. Influence of different structured channels of mesoporous silicate on the controlled ibuprofen delivery. *Asian J. Pharm. Sci.* **2017**, *12*, 418−423.
(42) Dziadkowiec, J.; Mansa, R.; Quintela, A.; Rocha, F.; Detellier, C. Preparation, characterization and application in controlled release of Ibuprofen-loaded Guar Gum/Montmorillonite Bionanocomposites. *Appl. Clay Sci.* **2017**, *135*, 52−63.
(43) Gouda, R.; Baishya, H.; Qing, Z. Application of mathematical models in drug release kinetics of carbidopa and levodopa ER tablets. *J. Dev. Drugs.* **2017**, *6*, 1−8.
(44) Ramteke, K. H.; Dighe, P. A.; Kharat, A. R.; Patil, S. V. Mathematical models of drug dissolution: a review. *Scholars Acad. J. Pharm.* **2014**, *3*, 388−396.

https://doi.org/10.1021/acsomega.1c01514
ACS Omega 2021, 6, 13406−13416